Molecular basis for amyloid-β polymorphism

Jacques-Philippe Colletier[a,1,2], Arthur Laganowsky[a,1,3], Meytal Landau[a,1], Minglei Zhao[a,1], Angela B. Soriaga[a,1], Lukasz Goldschmidt[a], David Flot[b], Duilio Cascio[a], Michael R. Sawaya[a], and David Eisenberg[a,4]

[a]Howard Hughes Medical Institute, Departments of Biological Chemistry and Chemistry and Biochemistry, UCLA-DOE Institute for Genomics and Proteomics, University of California, Los Angeles, CA 90095; and [b]European Synchrotron Radiation Facility, 6 rue Jules Horowitz, BP 220, 38043 Grenoble, France

Contributed by David Eisenberg, August 3, 2011 (sent for review June 13, 2011)

Amyloid-beta (Aβ) aggregates are the main constituent of senile plaques, the histological hallmark of Alzheimer's disease. Aβ molecules form β-sheet containing structures that assemble into a variety of polymorphic oligomers, protofibers, and fibers that exhibit a range of lifetimes and cellular toxicities. This polymorphic nature of Aβ has frustrated its biophysical characterization, its structural determination, and our understanding of its pathological mechanism. To elucidate Aβ polymorphism in atomic detail, we determined eight new microcrystal structures of fiber-forming segments of Aβ. These structures, all of short, self-complementing pairs of β-sheets termed steric zippers, reveal a variety of modes of self-association of Aβ. Combining these atomic structures with previous NMR studies allows us to propose several fiber models, offering molecular models for some of the repertoire of polydisperse structures accessible to Aβ. These structures and molecular models contribute fundamental information for understanding Aβ polymorphic nature and pathogenesis.

amyloid aggregation | 3D profile | protofilaments | heterotypic zipper

The amyloid hypothesis (1, 2) was based on the observation that amyloid-beta (Aβ), a 39–43 amino acid peptide that forms fibrillar, β-sheet rich structures, is the main constituent of proteinaceous deposits observed in the brains of Alzheimer's patients (3, 4). Evidence implicating Aβ in the pathogenesis of Alzheimer's disease includes the appearance of Alzheimer's symptoms in animal models that express the Aβ peptide (5) and the early onset of the disease coupled with massive depositions of Aβ in patients with the rare Aβ mutation, Asp23-to-Asn (Iowa mutant) (6). In vitro, the Aβ Iowa mutant forms fibers considerably faster than wild type (7). This finding that accelerated fiber formation is correlated to pathology points to fibers as the etiologic agent. In contrast, recent studies point to short fibers and soluble oligomeric forms of Aβ as the more toxic species (8–10). Thus it appears that different assemblies of Aβ are toxic, and they may share common structural features (11–13). Also supporting structural similarity of fibers and oligomers is the observation that many compounds, including analogs of the common amyloid ligands Congo red and thioflavin T, bind to both Aβ oligomers and fibers (14–17).

Despite decades of research, we lack full understanding of the molecular mechanisms of toxicity in Alzheimer's and other aggregation diseases. Part of the problem is the lack of structural information on the proteins mainly involved in the etiology, Aβ and Tau (3, 18). Atomic structures of oligomers of Aβ have been especially elusive due to their metastability and their heterogeneity in size and shape. More structural information is available for amyloid fibers, such as those associated with Alzheimer's disease and other aggregation diseases (19–35).

Different amyloid fibers display similar biophysical characteristics (36), most notably their common "cross-β structure" indicated by their X-ray fiber-diffraction patterns, displaying orthogonal reflections at about 4.8- and 10-Å spacings (37–39). The atomic features of the cross-β structure have been clarified by X-ray-derived atomic models of amyloid-like structures, revealing a motif consisting of a pair of tightly mated β-sheets, called a "steric zipper" (20). Steric zippers are formed from short self-complementary sequences and account for amyloid aggregation (20, 40, 41). These short peptide segments form well-ordered fibers (42) and have the biophysical characteristics of the fibers of their parent proteins (43). The structures of microcrystals of over 80 of these amyloid-like segments from different disease-associated proteins have been determined (44–49). These structures help to define cross-β structure, suggesting that stacks of identical short segments form the "cross-β spine" of the protofilament, the basic unit of the mature fiber, whereas the rest of the protein adopts either native-like or unfolded conformation peripheral to the spine (20, 50). Here, we hypothesize that steric zippers not only serve as the spine of the protofilament, but also can mediate the interactions between protofilaments that associate to form mature fibers.

Amyloid-forming proteins, and Aβ in particular, can display a bewildering variety of oligomeric and fiber forms, or *polymorphs* (27, 29, 31, 51–53). For example, Aβ_{1-40} was suggested to form five amyloid structures with distinct β-sheet contents and fiber stabilities (28). Experiment-based models of Aβ_{1-40} and Aβ_{1-42} described several fiber polymorphs. Solid-state (ss) NMR (ss-NMR) provided models for Aβ_{1-40} (21, 29, 31, 34, 35). A model for Aβ_{1-42} was derived using hydrogen-bonding constraints from quenched hydrogen/deuterium-exchange NMR, together with information from mutagenesis and previous ss-NMR studies (19). The models suggest that in these particular polymorphs, the Aβ molecule adopts a U-shaped protofilament structure, which hydrogen-bonds with identical molecules to form a pair of in-register, parallel β-sheets. However, the models differ in the precise location of the U-turn in the sequence, as well as in the specific interactions between distal regions, demonstrating that polymorphism is present at the protofilament level. Interestingly, the protofilament structure of Aβ_{1-40} fibers seeded from brain plaques was reported to differ from the earlier synthetic Aβ_{1-40} structures, with the C-terminal β-sheet flipped in relation to its interface with the N-terminal β-sheet (21, 34, 35). Tycko and cow-

Author contributions: J.-P.C., A.L., M.L., M.Z., A.B.S., L.G., and D.E. designed research; J.-P.C., A.L., M.L., M.Z., A.B.S., D.C., and M.R.S. performed research; L.G. and D.F. contributed new reagents/analytic tools; J.-P.C., A.L., M.L., M.Z., A.B.S., L.G., D.C., and M.R.S. analyzed data; and J.-P.C., A.L., M.L., M.Z., A.B.S., D.C., M.R.S., and D.E. wrote the paper.

The authors declare no conflict of interest.

Data deposition: The structures reported here (Tables S1 and S2) have been deposited in the Protein Data Bank, www.pdb.org [PDB ID codes 2Y2A (16-KLVFFA-21 Form I), 3OW9 (16-KLVFFA-21 Form II), 2Y29 (16-KLVFFA-21 Form III), 3Q2X (27-NKGAII-32), 3PZZ (29-GAIIGL-34), 2Y3J (30-AIIGLM-35), 2Y3K (35-MVGGVVIA-42 Form I), and 2Y3L (35-MVGGVVIA-42 Form II)].

[1]J.P.C, A.L., M.L., M.Z., and A.B.S. contributed equally to this work.

[2]Present address: (*i*) Institut de Biologie Structurale Jean-Pierre Ebel, Centre National de la Recherche Scientifique (Unité Mixte de Recherche 5075), Commissariat à l'Énergie Atomique, Université Joseph Fourier, 41 rue Jules Horowitz, 38027 Grenoble, France. (*ii*) Drug Discovery and Design Center, Shanghai Institute of Materia Medica, Chinese Academy of Sciences, Shanghai 201203, China.

[3]Present address: Department of Chemistry, University of Oxford, Chemistry Research Laboratory, Mansfield Road, Oxford, United Kingdom.

[4]To whom correspondence should be addressed. E-mail: david@mbi.ucla.edu.

This article contains supporting information online at www.pnas.org/lookup/suppl/doi:10.1073/pnas.1112600108/-/DCSupplemental.

orkers further expanded the range of structures available to Aβ by proposing an antiparallel protofilament structure for Asp23-to-Asn $A\beta_{1-40}$ (Iowa mutant) fibers; that is, successive stacked β-strands in each β-sheet run in opposite directions (7). Because all models reported so far were obtained from Aβ material that had been prepared by serial rounds of seeding, they presumably represent only a fraction of all conformations available to Aβ protofilaments. A higher level of polymorphism is manifested in varied modes of association of protofilaments into fibers (31, 34). For example, ss-NMR studies reported models for $A\beta_{1-40}$ fibers containing either two or three protofilaments (29). Finally, electron-density maps of Aβ fibers produced by cryoelectron microscopy displayed a variety of fiber forms (32, 51, 54, 55). It is interesting to note that in prion protein fibers, structural motifs other than tightly mated pairs of β-sheets were proposed. For example, an NMR-based model of HET-s(218–289) prion suggests a fiber formed via a β-solenoid triangular hydrophobic core (33).

The variety of polymorphs suggests that multiple interaction sites exist within each Aβ molecule, giving rise to differences in fiber morphologies and physicochemical properties on the surface of the fibers that may be correlated with varying levels of cellular toxicity (29, 31, 35, 56). This variety may provide an explanation for the poor correlation between the extent of amyloid deposition and the severity of neurological symptoms (4, 31, 57). Therefore, to better understand the nature of Aβ polymorphism in atomic detail, we report 8 previously undescribed crystal structures of Aβ segments that, together with three previously determined structures (45), span the sequence range $A\beta_{16-42}$. The 11 structures, all of which are steric zippers, reveal multiple modes of homotypic interactions (between identical segments), giving rise to a large variety of possible assemblies of Aβ molecules via different steric zipper spines. Combining our crystal structures of homotypic steric zippers with previous experiment-based models of Aβ, which suggest heterotypic interactions between distal segments in pairs of β-sheets (19, 21, 29, 34, 35), allows us to generate models of Aβ protofilament associations that exemplify the range of possible polymorphs.

Results

Identifying Fiber-Forming Segments in Aβ Using the 3D-Profile Method. We identified fiber-forming segments of Aβ predicted to form the spines of Aβ fibers (Fig. 1*A*). For this we used the 3D-profile method that scores six-residue sequence segments for their propensity to form steric zippers, based on the structural profile of a canonical steric zipper with a parallel, face-to-face, β-sheet orientation (for nomenclature, see ref. 45). Generally, the strands are allowed to translate in respect to each other, but the orientation of the strands (parallel vs. antiparallel) remains fixed (41, 59). Several segments within the regions of $A\beta_{11-25}$ and $A\beta_{27-42}$ were predicted either to self-associate into homotypic steric zippers (Fig. 1*A*) or to form heterotypic steric zippers in which one of the two β-sheets is composed of one segment and the complementary β-sheet is composed of a second segment (Fig. 1*C*). These predicted heterotypic interactions correlate with ss-NMR studies of $A\beta_{1-40}$ (21, 29) and an experiment-based model of $A\beta_{1-42}$ (19). In addition, the predicted heterotypic interactions within the $A\beta_{27-42}$ region correlate with a conformation of the $A\beta_{28-42}$ segment when fused to the C-terminal region of RNase (60). In this crystal structure, $A\beta_{28-42}$ forms a small antiparallel β-sheet with a bend formed by Gly37, yielding heterotypic interaction between residues 30–36 and 38–42, similar to the predictions of the 3D-profile method (Fig. 1*C*).

Crystal Structures of Six to Eight Residue Segments of Aβ. The 3D-profile method predicted several six-residue segments to be amyloidogenic (Fig. 1*A*). We examined these segments, as well as longer segments, for their ability to form fibers and crystals. Five segments ($A\beta_{16-21}$, $A\beta_{27-32}$, $A\beta_{29-34}$, $A\beta_{30-35}$, and $A\beta_{35-42}$) formed

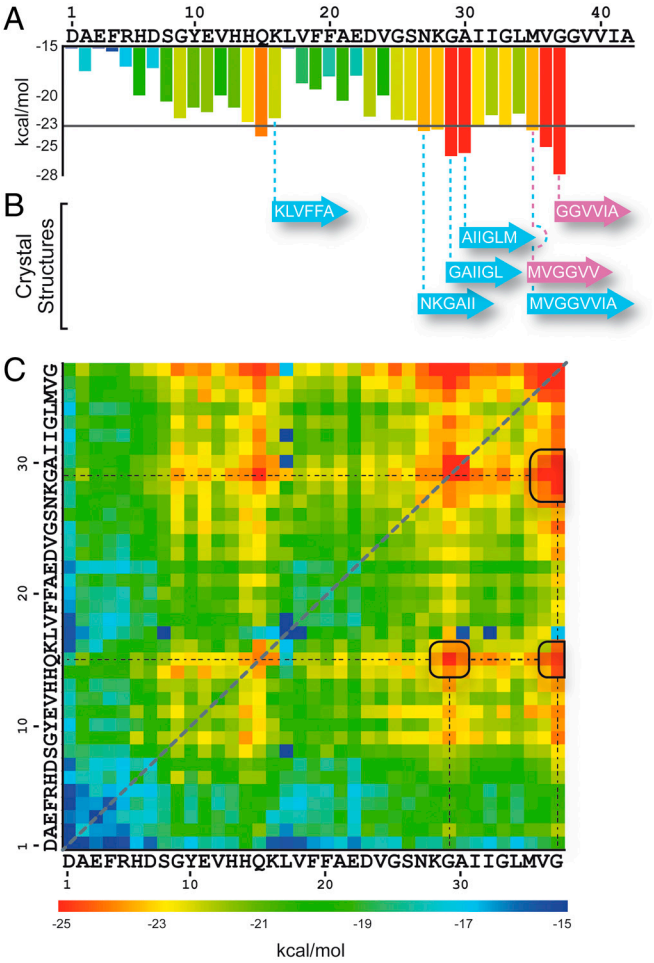

Fig. 1. Amyloidogenic propensity of Aβ homotypic and heterotypic interactions predicted by the 3D-profile method. (*A*) The 3D-profile method calculates the RosettaDesign energy (58) for the self-association (homotypic interactions) of six amino acid peptide segments (41, 59). The histogram of peptide segments is colored in rainbow from blue to red for segments with low-to-high predicted amyloid propensity. The Aβ amino acid sequence and residue numbering are shown (*Top*). (*B*) Aβ segments whose crystal structures have been determined are shown as arrows; blue and purple code for structures presented here or in a previous publication (45), respectively. (*C*) The 3D-profile method prediction for the association of hetero- and homo-Aβ segments is presented on a 2D-interaction heat map colored as in *A*. Each element represents the interaction energy of the hypothetical steric zipper of six residues that starts at the residues at the corresponding positions on the axes. Three main cross-peaks predicting high fiber-formation propensity are boxed.

microcrystals, with some forming more than a single crystal form (Fig. 2). Other segments suffered from low solubility or fast fibrillation, limiting their structural characterization to fiber diffraction and electron microscopy, as described below.

Previously, we described eight classes of steric zipper symmetries (45). Together, the steric zippers of Aβ presented here (Table S1) and in a previous publication (45) occupy six of these eight classes, suggesting the variety of possible arrangements of Aβ associations via different spine packings. We find both parallel and antiparallel packing of β-strands within β-sheets, as detailed in the following.

Crystal structures of the Aβ ^{16}KLVFFA^{21} segment. The $A\beta_{16-21}$ segment crystallized in three crystal forms (Fig. 2 *A–C*), all displaying an antiparallel β-strand stacking of the type "face=back" (45). That is, the β-sheets are equifacial, with identical side chains at the face and back of the β-sheet, a consequence of an internal

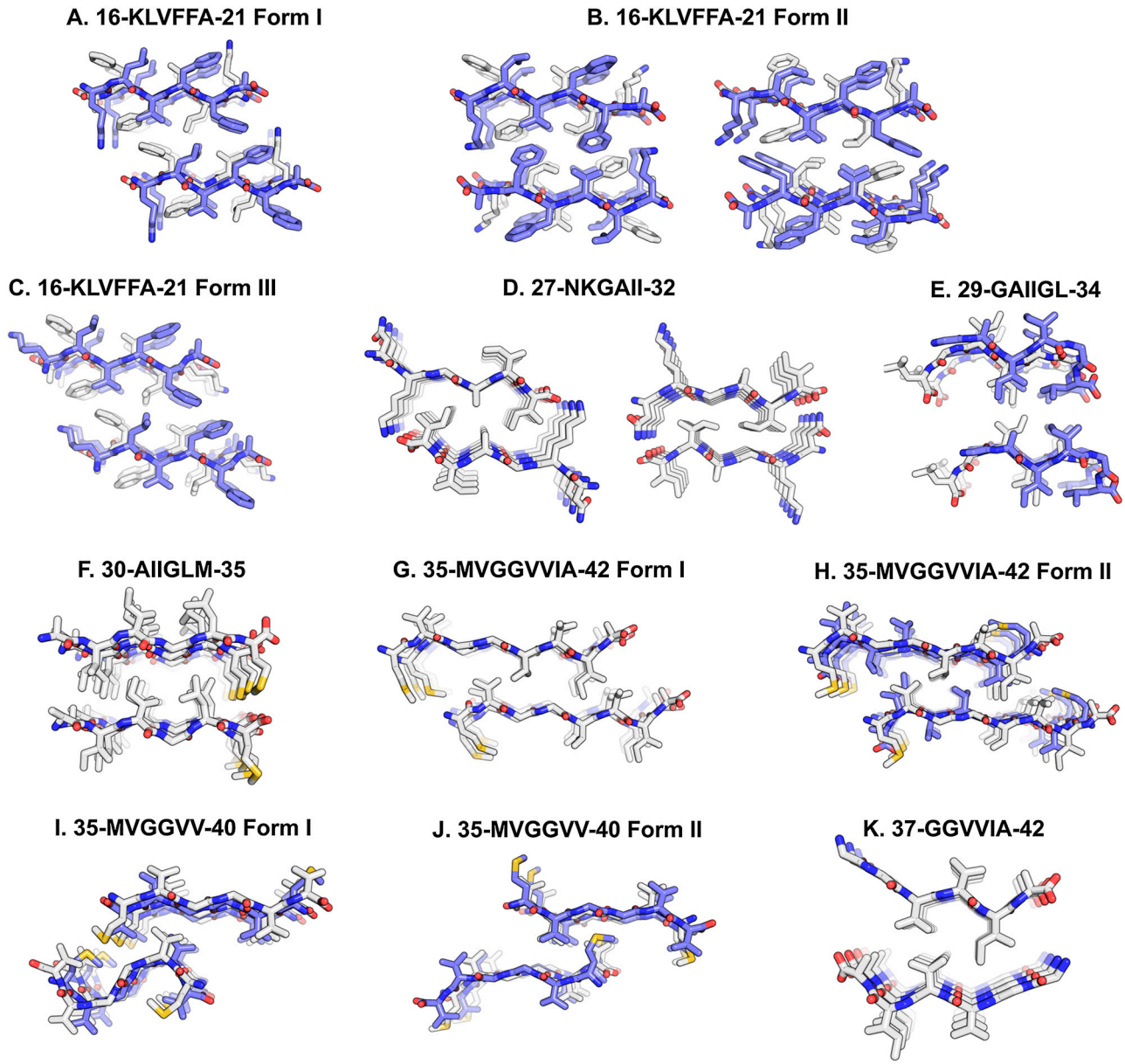

Fig. 2. Crystal structures of Aβ segments, shown in projection down the fiber axes. The Aβ segments are packed as pairs of interdigitated β-sheets, generally with a dry interface between them, termed steric zippers, forming the basic unit of the fiber (44, 45). The view here looks down the fiber axis, showing only four layers of β-strands in each β-sheet; actual fibers can contain more than 100,000 layers. Each panel is labeled with the amino acid sequence of each segment and the starting and ending residue numbers. Molecules are shown as sticks with noncarbon atoms colored by atom type. In structures with β-sheets composed of parallel strands (*D*, *F*, *G*, and *K*), the carbons are in white. Antiparallel strands forming β-sheet structures (*A–C*, *E*, *H–J*) are alternately colored with carbons colored white and blue. Closest partners across the dry interface share the same color. Some of the panels are split in two halves; each half represents a different dry interface within the same crystal structure.

twofold screw symmetry element. $A\beta_{16-21}$ forms I and III (Fig. 2*A* and *C*) display similar interfaces with different conformations of Lys16, and a slight registration slip of the steric zipper interface. $A\beta_{16-21}$ form II displays two steric zipper interfaces that differ in rotamer conformation of Phe20 (Fig. 2*B*). In all zippers, the pairs of β-sheets are packed together via hydrophobic side chains, forming a dry interface. All four steric zippers belong to symmetry class 7 (45).

Corresponding to our structures, ss-NMR characterization of a one-residue longer peptide, $A\beta_{16-22}$ (26), as well as a one-residue shorter peptide, $A\beta_{17-21}$ (30), showed an antiparallel organization of β-sheets in the fibers. Fibers of longer segments, $A\beta_{11-25}$ (30) and $A\beta_{34-42}$ (61), also display an antiparallel β-strand orientation. The antiparallel orientation might be associated with pathology seeing that it was observed for a subset of fibers of the "Iowa" Aβ mutant that is related to a familial, early onset, Alzheimer's disease (6, 7). In addition, Aβ oligomers were also suggested to form antiparallel β-sheet structures (62–65). In contrast, the wild-type, full-length Aβ fibers display a parallel orientation (25).

Crystal structure of the Aβ ^{27}NKGAII^{32} segment. The $A\beta_{27-32}$ segment forms a parallel β-sheet stacking with two different steric zipper interfaces. Both interfaces show β-sheets packed together via interdigitating hydrophobic side chains, typical of symmetry class 1 (45). One interface shows a "face-to-face" orientation and the other "back-to-back" (Fig. 2*D*).

Crystal structure of the Aβ ^{29}GAIIGL^{34} segment. The $A\beta_{29-34}$ segment forms an antiparallel β-sheet with a dry steric zipper

interface displaying a "face-to-back" orientation (Fig. 2*E*). The two nonequifacial antiparallel β-sheets are related to each other by a simple translation vector, corresponding to symmetry class 6 (45). The registration between neighboring antiparallel strands is such that the last two residues in each strand fall outside the hydrogen-bonding pattern of the β-sheet. Specifically, Gly33 deviates from β-sheet geometry, placing Leu34 outside the β-sheet. The conformation of Gly33 and Leu34 are different in the two antiparallel strands in the asymmetric unit, which correspond to neighboring strands within the β-sheet.

Crystal structure of the Aβ ^{30}AIIGLM^{35} segment. The A$\beta_{30–35}$ segment forms a parallel β-sheet with a dry steric zipper interface of the type face-to-back, symmetry class 2 (Fig. 2*F*). This steric zipper interface resembles a "knobs-into-holes" type of packing (66); i.e., Ile32 and Leu34 from one β-sheet form the "knob" that enters the "hole" between Ile31 and Met35 of the mating β-sheet, created by the presence of Gly33 (lacking a side chain).

Crystal structures of the Aβ ^{35}MVGGVVIA^{42} segment. The A$\beta_{35–42}$ segment crystallized in two crystal forms displaying both parallel (face-to-back orientation, symmetry class 2) (Fig. 2*G*) and antiparallel (face = back orientation, symmetry class 7) (Fig. 2*H*) β-sheet stacking. Interestingly, the two steric zippers display a similar interface with minor conformation differences of side chains, and a knobs-into-holes type of packing similar to that described for A$\beta_{30–35}$. The knob is formed by Val39 and Ile41 that accommodate the hole formed by the presence of glycine residues.

Previously described structures of A$\beta_{35–40}$ and A$\beta_{37–42}$ segments (45) are shown in Figure 2 *I–K*. A$\beta_{35–40}$ crystallized in two forms, both displaying antiparallel β-sheets with a face = back orientation, symmetry class 8 (Fig. 2 *I–J*). A$\beta_{37–42}$ forms parallel β-sheets with a face-to-back orientation, symmetry class 4 (Fig. 2*K*).

Quasicrystalline Fibers of Long (11–20 Residue) Aβ Segments. Our attempts to crystallize longer segments of Aβ (A$\beta_{11–25}$, A$\beta_{16–35}$, A$\beta_{22–35}$, and A$\beta_{30–42}$) resulted in highly disordered microcrystals. The X-ray diffraction patterns (Fig. S1) show a mix of crystalline and fiber diffraction, termed *quasicrystalline fiber diffraction* (67). These diffraction patterns display a distinguishable feature at reciprocal spacing of 4.8 Å, which is consistent with parallel, in-register, β-sheet structures. A feature at a spacing of 9.6 Å, expected for either antiparallel β-sheets or out-of-register parallel β-sheets, is not present.

Fiber Formation of Aβ Segments Analyzed by Electron Microscopy. We examined the fiber-forming propensities of Aβ segments, including 6–8 residue segments that form microcrystals (A$\beta_{16–21}$, A$\beta_{30–35}$, A$\beta_{35–40}$, A$\beta_{35–42}$, and A$\beta_{37–42}$) (Fig. S2*A*), as well as 11–20 residue segments (A$\beta_{11–25}$, A$\beta_{16–35}$, A$\beta_{30–40}$, and A$\beta_{30–42}$) (Fig. S3*A*). All of the Aβ segments formed fibers. It is noteworthy that A$\beta_{30–35}$ forms small microcrystals even under fibrillation conditions, and fibers can grow from the tip of microcrystals (Fig. S2*A*), suggesting common structural features for fibers and microcrystals (48).

Can Distal Aβ Segments Associate to Form the Spine Structures of Amyloid Fibers? Identification of fiber-forming segments in Aβ using the 3D-profile method predicted the association of distal segments to form heterotypic steric zippers (Fig. 1*C*). Based on these predictions, we carried out cocrystallization screens of 1:1 mixtures of distal peptide segments (A$\beta_{16–21}$ + A$\beta_{30–35}$, A$\beta_{16–21}$ + A$\beta_{35–40}$, A$\beta_{16–21}$ + A$\beta_{35–42}$, A$\beta_{16–21}$ + A$\beta_{37–42}$, A$\beta_{11–25}$ + A$\beta_{30–40}$, A$\beta_{15–25}$ + A$\beta_{30–40}$, A$\beta_{11–25}$ + A$\beta_{30–42}$, and A$\beta_{15–25}$ + A$\beta_{30–42}$), but failed to produce diffracting crystals containing two differing peptide segments. Nonetheless, electron micrographs of fibers grown from certain mixtures display a morphology that is distinct from the morphologies of the individual segments (Figs. S2*B* and S3*B*).

Discussion

Aβ, as well as several of its peptide segments, readily forms fibers (Figs. S2 and S3) (4). Eleven short segments (6–8 residues) also form microcrystals permitting us to determine their structures in atomic detail (Fig. 2). These structures represent 13 diverse steric zipper interfaces, each of which can serve as the spine for fiber formation (20). In previous work, we termed this phenomenon *segmental polymorphism* (48).

Types of Amyloid Polymoprhism. Four steric zipper structures (A$\beta_{16–21}$, A$\beta_{27–32}$, A$\beta_{35–40}$, and A$\beta_{35–42}$) show a second type of amyloid polymorphism, termed *packing polymorphism*, in which the same sequence can form distinct steric zipper structures by virtue of different packing in the spine (48) (Fig. 2). A$\beta_{35–42}$ shows a previously undescribed mode of packing polymorphism, with β-sheets stacking via both parallel and antiparallel β-strands (Fig. 2 *G* and *H*). Of particular importance, this previously undescribed type of polymorphism may be related to Aβ toxicity. The Aβ Iowa mutation (Asp23-to-Asn) (6) is the determinant for familial, early onset, Alzheimer's disease. The majority of fibers formed from the mutant A$\beta_{1–40}$ suggest an antiparallel orientation (7) and deposit massively compared to wild-type Aβ fibers, which exclusively exhibit a parallel orientation (25). Of interest, the two types of polymorphs (parallel vs. antiparallel) were observed within the same sample of the Iowa mutant A$\beta_{1–40}$ (7). This observation can be explained structurally by our crystal structures. Two different polymorphs of A$\beta_{35–42}$ showing parallel and antiparallel β-sheet orientation nevertheless show similar interfaces of the two steric zippers with only slightly dissimilar side-chain conformations (Fig. 2 *G* and *H*). Also, antiparallel β-sheet structures have been reported for Aβ oligomers (62–65), which recent studies point as more toxic than fibers (8–10).

The steric zipper structures of Aβ segments (Fig. 2), as well as of segments from other disease-related amyloid proteins (44–49), all show homotypic interactions, with the pair of β-sheets formed from the same segment of the protein. Heterotypic interactions, between β-sheets formed from different Aβ segments, were proposed based on NMR studies (19, 21) and the interpretation of cryoelectron microscopy maps (32, 51, 54, 55). Our predictions, based on the 3D-profile method, suggest the association of distal segments to form heterotypic steric zippers (Fig. 1*C*). Our observations of fiber formation of the different Aβ segments are compatible with this notion, as fibers formed from mixed pairs of Aβ segments display different morphologies compared to fibers formed from individual segments (Figs. S2 and S3). The heterotypic interactions suggest a fourth mode of amyloid polymorphism, *heterotypic polymorphism*, which is an example of *combinatorial polymorphism* suggested in previous work (48). With the numerous modes of segmental, packing, and heterotypic polymorphism available for fiber formation, a given Aβ fiber may contain more than a single type of protofilament, each displaying a different kind of polymorphism, as discussed in the following.

Pseudoatomic Aβ Fiber Models. Using our atomic structures of steric zippers of Aβ segments, combined with models of the protofilament structure (19, 34), we constructed several atomic models of Aβ fibers that exemplify the numerous possibilities for fiber morphology (Fig. 3 and Figs. S4–S6). The protofilament models, namely pairs of tightly mating β-sheets, one of A$\beta_{1–40}$ derived from ss-NMR studies (34), and another of an experiment-based model of A$\beta_{1–42}$ (19), show a U-shaped structure. In A$\beta_{1–40}$, residues 23–29 form a bend in the backbone to bring two β-sheets, composed of residues 10–22 and 30–40, to form a heterotypic interface (34). In A$\beta_{1–42}$, the heterotypic interactions

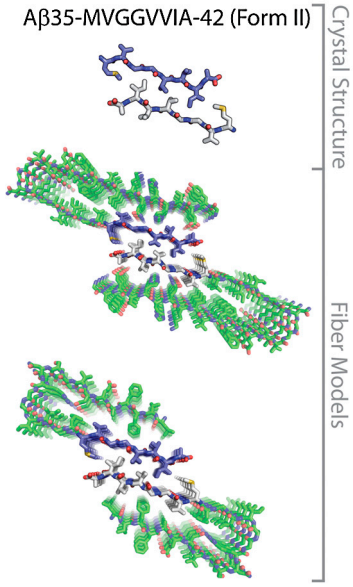

Fig. 3. Models of protofilament associations. The crystal structure of Aβ35-42 Form II was used to model interactions between two protofilaments. The protofilament structure is derived from experiment-based models of Aβ1-40 (residues 1–9 are disordered in the fiber) (34) (*Upper*) or Aβ1-42 (residues 1–17 are disordered in the fiber) (19) (*Lower*). See also Figs. S4–S6 for other models of Aβ polymorphs based on the structures of Fig. 2.

are between β-sheets formed by residues 18–26 and 31–42 (19). Few examples of Aβ fiber models are constructed from the steric zipper structures of $A\beta_{35–42}$, $A\beta_{16–21}$, or $A\beta_{27–32}$ mediating the interactions between the two different types of protofilaments (Fig. 3 and Fig. S4). The interprotofilament interface suggested by the model of Fig. S4*A* differs from those of Fig. 3 and Fig. S4*B* and involves the pairing of the N-terminal β-sheets for the former and the pairing of the C-terminal β-sheets for the latter. A quaternary model that includes the association of the C-terminal β-sheets was previously suggested by ss-NMR studies (34). The interprotofilament interface in this NMR model covers residues 30–40, which is longer than the interfaces of Fig. 3 and Fig. S4*B*, which cover residues 35–42 or 27–32, respectively, and thus might represent a more stable polymorph.

Overall, our models (Fig. 3 and Fig. S4) incorporate different segments as the spines, exemplifying segmental polymorphism. They display diverse interfaces within the fiber, incorporating variation within the protofilament structure, as suggested by experiments (19, 34), as well as variation in the interactions between protofilaments composing the mature fiber. Additional fiber models displaying the association of multiple protofilaments via several different core regions illustrate a higher level of segmental polymorphism (Fig. S5).

Our predictions of fiber-forming segments show a cluster of predicted interactions within residues 30–42 of Aβ (Fig. 1*C*). Structures of segments within this region, of $A\beta_{30–35}$ and $A\beta_{35–42}$, show steric zippers forming a knobs-into-holes type of packing (66) (Fig. 2 *F–H*). Correspondingly, we modeled a steric zipper that is longer than those determined by the crystal structures and spans residues 31–42, displaying a similar kind of knobs-into-holes packing between two protofilaments (Fig. S6*A*). In this longer model, residues Val39 and Ile41 protrude into the void created by Gly33, and Met35 protrudes into the void created by Gly37-Gly38, similar to the structure of $A\beta_{35–40}$ (Fig. 2*J*). The NMR-based quaternary model of $A\beta_{1–40}$ (34) displays a similar, but slightly shifted, knobs-into-holes interface, with Ile31 forming the knob that protrudes into the void created by Gly37-Gly38, and Met35 forming the knob that protrudes into the void created by Gly33. Finally, in order to demonstrate polymorphism that is associated with the disease-related Iowa Aβ mutant (6, 7), we constructed a fiber model based on the crystal structure of $A\beta_{16–21}$ displaying an antiparallel orientation (Fig. S6*B*).

Our results offer a molecular basis for amyloid polymorphism. Thirteen different steric zipper interfaces display a variety of polymorphic arrangements (Fig. 2). By combining our crystal structures with previous NMR studies, we offer fiber models that illustrate the structural variety of Aβ assemblies. Polymorphism produces a variety of structures with a variety of cellular toxicities, and a molecular view into the different structures may advance our understanding of the mechanisms of amyloid toxicity.

Materials and Methods

Materials. Peptide segments (custom synthesis, minimal purity of 98%) were purchased from CS Bio. Chemicals were purchased from Thermo-Fisher and Sigma-Aldrich.

Crystallization Conditions. All crystals were grown at 18 °C via hanging-drop vapor diffusion. Details of crystallization, structure determination, and refinement are provided in *SI Text*.

Modeling of Full-Length Aβ Fibers. Models of Aβ fibers were contracted based on experiment-based models of $A\beta_{1–40}$ and $A\beta_{1–42}$ protofilaments (19, 34) aligned with the steric zipper interfaces and refined as described in *SI Text*.

Fiber Formation Assessed by Electron Microscopy. Samples were prepared as described in *SI Text*.

ACKNOWLEDGMENTS. This work is based upon research conducted at the Northeastern Collaborative Access Team beamlines of the Advanced Photon Source (APS) and the ID23-EH2 beamline at the European Synchrotron Radiation Facility (ESRF). We appreciatively acknowledge ESRF and APS for beamtime and the staffs for help during data collection. J.P.C. is recipient of the International Young Researcher fellowship from the Chinese Academy of Science. We thank National Institutes of Health, Department of Energy, and Howard Hughes Medical Institute for support.

1. Hardy JA, Higgins GA (1992) Alzheimer's disease: The amyloid cascade hypothesis. *Science* 256:184–185.
2. Selkoe DJ (1991) Alzheimer's disease. In the beginning. *Nature* 354:432–433.
3. Glenner GG, Wong CW, Quaranta V, Eanes ED (1984) The amyloid deposits in Alzheimer's disease: Their nature and pathogenesis. *Appl Pathol* 2:357–369.
4. Selkoe DJ (1994) Alzheimer's disease: A central role for amyloid. *J Neuropathol Exp Neurol* 53:438–447.
5. Ashe KH, Zahs KR (2010) Probing the biology of Alzheimer's disease in mice. *Neuron* 66:631–645.
6. Van Nostrand WE, Melchor JP, Cho HS, Greenberg SM, Rebeck GW (2001) Pathogenic effects of D23N Iowa mutant amyloid beta-protein. *J Biol Chem* 276:32860–32866.
7. Tycko R, Sciarretta KL, Orgel JP, Meredith SC (2009) Evidence for novel beta-sheet structures in Iowa mutant beta-amyloid fibrils. *Biochemistry* 48:6072–6084.
8. Lambert MP, et al. (1998) Diffusible, nonfibrillar ligands derived from Abeta1-42 are potent central nervous system neurotoxins. *Proc Natl Acad Sci USA* 95:6448–6453.
9. Lesne S, et al. (2006) A specific amyloid-beta protein assembly in the brain impairs memory. *Nature* 440:352–357.
10. Xue WF, Hellewell AL, Hewitt EW, Radford SE (2010) Fibril fragmentation in amyloid assembly and cytotoxicity: When size matters. *Prion* 4:20–25.
11. Collins SR, Douglass A, Vale RD, Weissman JS (2004) Mechanism of prion propagation: Amyloid growth occurs by monomer addition. *PLoS Biol* 2:e321.
12. Chimon S, et al. (2007) Evidence of fibril-like beta-sheet structures in a neurotoxic amyloid intermediate of Alzheimer's beta-amyloid. *Nat Struct Mol Biol*.
13. Ono K, Condron MM, Teplow DB (2009) Structure-neurotoxicity relationships of amyloid β-protein oligomers. *Proc Natl Acad Sci USA* 106:14745–14750.
14. Maezawa I, et al. (2008) Congo red and thioflavin-T analogs detect Abeta oligomers. *J Neurochem* 104:457–468.
15. Necula M, Kayed R, Milton S, Glabe CG (2007) Small molecule inhibitors of aggregation indicate that amyloid beta oligomerization and fibrillization pathways are independent and distinct. *J Biol Chem* 282:10311–10324.
16. Hong HS, et al. (2007) Combining the rapid MTT formazan exocytosis assay and the MC65 protection assay led to the discovery of carbazole analogs as small molecule inhibitors of Abeta oligomer-induced cytotoxicity. *Brain Res* 1130:223–234.
17. Yang F, et al. (2005) Curcumin inhibits formation of amyloid beta oligomers and fibrils, binds plaques, and reduces amyloid in vivo. *J Biol Chem* 280:5892–5901.
18. Steiner B, et al. (1990) Phosphorylation of microtubule-associated protein tau: Identification of the site for Ca2(+)-calmodulin dependent kinase and relationship with tau phosphorylation in Alzheimer tangles. *EMBO J* 9:3539–3544.

19. Luhrs T, et al. (2005) 3D structure of Alzheimer's amyloid-beta(1-42) fibrils. *Proc Natl Acad Sci USA* 102:17342–17347.
20. Nelson R, Eisenberg D (2006) Recent atomic models of amyloid fibril structure. *Curr Opin Struct Biol* 16:260–265.
21. Petkova AT, et al. (2002) A structural model for Alzheimer's beta-amyloid fibrils based on experimental constraints from solid state NMR. *Proc Natl Acad Sci USA* 99:16742–16747.
22. Bayro MJ, et al. (2010) High-resolution MAS NMR analysis of PI3-SH3 amyloid fibrils: Backbone conformation and implications for protofilament assembly and structure. *Biochemistry* 49:7474–7484.
23. Greenwald J, et al. (2010) The mechanism of prion inhibition by HET-S. *Mol Cell* 38:889–899.
24. Shewmaker F, Wickner RB, Tycko R (2006) Amyloid of the prion domain of Sup35p has an in-register parallel beta-sheet structure. *Proc Natl Acad Sci USA* 103:19754–19759.
25. Antzutkin ON, et al. (2000) Multiple quantum solid-state NMR indicates a parallel, not antiparallel, organization of beta-sheets in Alzheimer's beta-amyloid fibrils. *Proc Natl Acad Sci USA* 97:13045–13050.
26. Balbach JJ, et al. (2000) Amyloid fibril formation by A beta 16–22, a seven-residue fragment of the Alzheimer's beta-amyloid peptide, and structural characterization by solid state NMR. *Biochemistry* 39:13748–13759.
27. Goldsbury C, et al. (2000) Amyloid fibril formation from full-length and fragments of amylin. *J Struct Biol* 130:352–362.
28. Kodali R, Williams AD, Chemuru S, Wetzel R (2010) Abeta(1-40) forms five distinct amyloid structures whose beta-sheet contents and fibril stabilities are correlated. *J Mol Biol* 401:503–517.
29. Paravastu AK, Leapman RD, Yau WM, Tycko R (2008) Molecular structural basis for polymorphism in Alzheimer's beta-amyloid fibrils. *Proc Natl Acad Sci USA* 105:18349–18354.
30. Petkova AT, et al. (2004) Solid state NMR reveals a pH-dependent antiparallel beta-sheet registry in fibrils formed by a beta-amyloid peptide. *J Mol Biol* 335:247–260.
31. Petkova AT, et al. (2005) Self-propagating, molecular-level polymorphism in Alzheimer's beta-amyloid fibrils. *Science* 307:262–265.
32. Sachse C, Fandrich M, Grigorieff N (2008) Paired beta-sheet structure of an Abeta(1-40) amyloid fibril revealed by electron microscopy. *Proc Natl Acad Sci USA* 105:7462–7466.
33. Wasmer C, et al. (2008) Amyloid fibrils of the HET-s(218-289) prion form a beta solenoid with a triangular hydrophobic core. *Science* 319:1523–1526.
34. Petkova AT, Yau WM, Tycko R (2006) Experimental constraints on quaternary structure in Alzheimer's beta-amyloid fibrils. *Biochemistry* 45:498–512.
35. Paravastu AK, Qahwash I, Leapman RD, Meredith SC, Tycko R (2009) Seeded growth of beta-amyloid fibrils from Alzheimer's brain-derived fibrils produces a distinct fibril structure. *Proc Natl Acad Sci USA* 106:7443–7448.
36. Gazit E (2005) Mechanisms of amyloid fibril self-assembly and inhibition. Model short peptides as a key research tool. *FEBS J* 272:5971–5978.
37. Kirschner DA, Abraham C, Selkoe DJ (1986) X-ray diffraction from intraneuronal paired helical filaments and extraneuronal amyloid fibers in Alzheimer disease indicates cross-beta conformation. *Proc Natl Acad Sci USA* 83:503–507.
38. Astbury WT, Beighton E, Parker KD (1959) The cross-beta configuration in supercontracted proteins. *Biochim Biophys Acta* 35:17–25.
39. Sunde M, et al. (1997) Common core structure of amyloid fibrils by synchrotron X-ray diffraction. *J Mol Biol* 273:729–739.
40. Ivanova MI, Thompson MJ, Eisenberg D (2006) A systematic screen of beta(2)-microglobulin and insulin for amyloid-like segments. *Proc Natl Acad Sci USA* 103:4079–4082.
41. Thompson MJ, et al. (2006) The 3D profile method for identifying fibril-forming segments of proteins. *Proc Natl Acad Sci USA* 103:4074–4078.
42. Gazit E (2002) Mechanistic studies of the process of amyloid fibrils formation by the use of peptide fragments and analogues: Implications for the design of fibrillization inhibitors. *Curr Med Chem* 9:1725–1735.
43. Balbirnie M, Grothe R, Eisenberg DS (2001) An amyloid-forming peptide from the yeast prion Sup35 reveals a dehydrated beta-sheet structure for amyloid. *Proc Natl Acad Sci USA* 98:2375–2380.
44. Nelson R, et al. (2005) Structure of the cross-beta spine of amyloid-like fibrils. *Nature* 435:773–778.
45. Sawaya MR, et al. (2007) Atomic structures of amyloid cross-beta spines reveal varied steric zippers. *Nature* 447:453–457.
46. Wiltzius JJ, et al. (2008) Atomic structure of the cross-β spine of islet amyloid polypeptide (amylin). *Protein Sci* 17:1467–1474.
47. Apostol MI, Sawaya MR, Cascio D, Eisenberg D (2010) Crystallographic studies of prion protein (PrP) segments suggest how structural changes encoded by polymorphism at residue 129 modulate susceptibility to human prion disease. *J Biol Chem* 285:29671–29675.
48. Wiltzius JJ, et al. (2009) Molecular mechanisms for protein-encoded inheritance. *Nat Struct Mol Biol* 16:973–978.
49. Ivanova MI, Sievers SA, Sawaya MR, Wall JS, Eisenberg D (2009) Molecular basis for insulin fibril assembly. *Proc Natl Acad Sci USA* 106:18990–18995.
50. Sambashivan S, Liu Y, Sawaya MR, Gingery M, Eisenberg D (2005) Amyloid-like fibrils of ribonuclease A with three-dimensional domain-swapped and native-like structure. *Nature* 437:266–269.
51. Meinhardt J, Sachse C, Hortschansky P, Grigorieff N, Fandrich M (2009) Abeta(1-40) fibril polymorphism implies diverse interaction patterns in amyloid fibrils. *J Mol Biol* 386:869–877.
52. Andrews ME, Inayathullah NM, Jayakumar R, Malar EJ (2009) Conformational polymorphism and cellular toxicity of IAPP and beta AP domains. *J Struct Biol* 166:116–125.
53. Komatsu H, Feingold-Link E, Sharp KA, Rastogi T, Axelsen PH (2010) Intrinsic linear heterogeneity of amyloid β protein fibrils revealed by higher resolution mass-per-length determinations. *J Biol Chem* 285:41843–41851.
54. Schmidt M, et al. (2009) Comparison of Alzheimer Abeta(1-40) and Abeta(1-42) amyloid fibrils reveals similar protofilament structures. *Proc Natl Acad Sci USA* 106:19813–19818.
55. Zhang R, et al. (2009) Interprotofilament interactions between Alzheimer's Abeta1-42 peptides in amyloid fibrils revealed by cryoEM. *Proc Natl Acad Sci USA* 106:4653–4658.
56. Yoshiike Y, Akagi T, Takashima A (2007) Surface structure of amyloid-beta fibrils contributes to cytotoxicity. *Biochemistry* 46:9805–9812.
57. Kirkitadze MD, Bitan G, Teplow DB (2002) Paradigm shifts in Alzheimer's disease and other neurodegenerative disorders: The emerging role of oligomeric assemblies. *J Neurosci Res* 69:567–577.
58. Kuhlman B, Baker D (2000) Native protein sequences are close to optimal for their structures. *Proc Natl Acad Sci USA* 97:10383–10388.
59. Goldschmidt L, Teng PK, Riek R, Eisenberg D (2010) Identifying the amylome, proteins capable of forming amyloid-like fibrils. *Proc Natl Acad Sci USA* 107:3487–3492.
60. Takano K, et al. (2006) Structure of amyloid beta fragments in aqueous environments. *FEBS J* 273:150–158.
61. Lansbury PT, Jr, et al. (1995) Structural model for the beta-amyloid fibril based on interstrand alignment of an antiparallel-sheet comprising a C-terminal peptide. *Nat Struct Biol* 2:990–998.
62. Cerf E, et al. (2009) Antiparallel beta-sheet: A signature structure of the oligomeric amyloid beta-peptide. *Biochem J* 421:415–423.
63. Yu L, et al. (2009) Structural characterization of a soluble amyloid beta-peptide oligomer. *Biochemistry* 48:1870–1877.
64. Eckert A, et al. (2008) Oligomeric and fibrillar species of beta-amyloid (A beta 42) both impair mitochondrial function in P301L tau transgenic mice. *J Mol Med* 86:1255–1267.
65. Habicht G, et al. (2007) Directed selection of a conformational antibody domain that prevents mature amyloid fibril formation by stabilizing Abeta protofibrils. *Proc Natl Acad Sci USA* 104:19232–19237.
66. Crick FH (1952) Is alpha-keratin a coiled coil? *Nature* 170:882–883.
67. Rousseau F, Schymkowitz J, Serrano L (2006) Protein aggregation and amyloidosis: confusion of the kinds? *Curr Opin Struct Biol* 16:118–126.